AIP | The Journal of Chemical Physics

Metallic nanoparticles meet metadynamics

L. Pavan, K. Rossi, and F. Baletto

Citation: The Journal of Chemical Physics **143**, 184304 (2015); doi: 10.1063/1.4935272
View online: http://dx.doi.org/10.1063/1.4935272
View Table of Contents: http://scitation.aip.org/content/aip/journal/jcp/143/18?ver=pdfcov
Published by the AIP Publishing

Metallic nanoparticles meet metadynamics

L. Pavan, K. Rossi, and F. Baletto[a)]
Physics Department, King's College London, London WC2R 2LS, United Kingdom

(Received 12 July 2015; accepted 26 October 2015; published online 11 November 2015)

Metadynamics coupled with classical molecular dynamics has been successfully applied to sample the configuration space of metallic and bimetallic nanoclusters. We implement a new set of collective variables related to the pair distance distribution function of the nanoparticle to achieve an exhaustive isomer sampling. As paradigmatic examples, we apply our methodology to Ag_{147}, Pt_{147}, and their alloy $Ag^{shell}Pt^{core}$ at 2:1 and 1:1 chemical compositions. The proposed scheme is able to reproduce the known solid-solid structural transformation pathways, based on the Lipscomb's diamond-square-diamond mechanisms, both in mono and bimetallic nanoparticles. A discussion of the free energy barriers involved in these processes is provided. © *2015 AIP Publishing LLC.* [http://dx.doi.org/10.1063/1.4935272]

I. INTRODUCTION

Mono and bimetallic nanoparticles (NPs) find a wide number of applications ranging from catalysis and biomedicine to optoelectronics and magnetic data storage due to their high surface to volume ratio, peculiar shape, and *d*-band shift.[1,2] Nanoclusters' chemophysical properties strongly depend on the interplay between their size, morphology, and chemical composition. Understanding the thermal stability of an isomer, including complex entropic contributions difficult to be addressed experimentally,[3] is highly desirable and many theoretical attempts have been presented in the literature to tackle this problem.[4–6] The investigation of the solid-solid structural pathways and the evaluation of their free energy barriers (FEBs) may shed light on how cluster's chemical features vary due to ageing and external factors such as temperature or pressure. Although recent developments made possible the detection of solid-solid transformations via electron beam irradiation,[7,8] only numerical approaches can give insights on the atomistic details and provide an accurate sampling of energy landscapes.[9]

Numerical tools to obtain a quantitative sampling of the conformational space of a system can be divided in two families. Double ended search methods are based upon the *a priori* knowledge of the initial and final point of the transition. These techniques evaluate the minimum energy path, using an eigenvector-following algorithm to determine the saddle point and then a steepest-descent energy minimisation to identify the lowest energy mechanism. Notable examples are the nudged elastic band[10] and the double-ended transition path sampling (DETPS).[11] Double ended approaches have been applied to a wide range of systems which also include bimetallic nanoclusters.[12] However, these calculations become expensive when used to analyse structural rearrangements in systems with high friction, high free energy barriers, or a very rough free energy landscape.[13] Temperature accelerated and biased sampling techniques represent the other approach: an initial configuration of the system is excited or perturbed and forced to visit new and unknown isomers. Metadynamics,[14,15] adaptive biasing force,[16] umbrella sampling,[17] and parallel tempering[18] are all renown techniques based upon this idea. Perturbation methods have been commonly used to detect order-disorder transition while rarely to simulate solid-solid structural transformations in nanoalloys.[19–24]

In this paper, we demonstrate how Metadynamics (MetaD) can be successfully employed to sample the configuration space of relatively large metallic and bimetallic nanoparticles at finite temperatures. MetaD algorithm coarses the system dynamics in a collective variables (CVs) space where a history dependent potential is exploited to accelerate rare events as minimum-minimum transitions. It further allows to reconstruct the system's free energy surface (FES) projection in the CV space.[14,15] This method has been applied to finite inorganic nanosystems such as semiconductor/quantum dots,[25,26] alkali halides,[27,28] and Lennard-Jones.[29,30] However, it has been applied only to metallic nanoclusters with less than 20 atoms[31,32] and never to bimetallic systems. Our MetaD scheme, with CVs being window functions on the pair distance distribution function, reproduces the well known five and six diamond-square-diamond (DSD)[33,34] mechanisms in both mono and bimetallic systems. Moreover, Mackay's prediction of the transformation of an icosahedron into an anticuboctahedron (aCo) has been proven numerically for the first time.

Section II reports the methodology adopted to explore the NP free energy landscape, Sec. III contains a focus on the descriptions of the structural pathways detected during our MetaD runs, followed by a quantitative analysis of energy barriers. A resumé of our results and discussion is presented in Sec. IV.

II. MODELS AND METHOD

We consider monometallic (Ag,Pt) and bimetallic (AgPt) nanoparticles at 2:1 and 1:1 chemical composition, made of 147 atoms. At this size, noble and quasi-noble metals are likely to assume closed shell polyhedra shapes. The most

a)Electronic mail: francesca.baletto@kcl.ac.uk

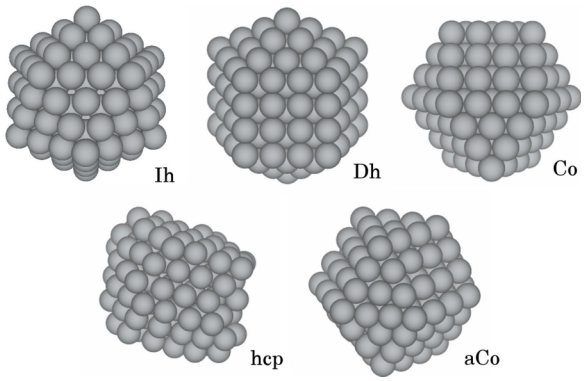

FIG. 1. Closed shell polyhedra at 147 atoms. From left to right, top row: icosahedron, decahedron, cuboctahedron. Bottom row: hexagonal closed packed and anticuboctahedron.

common are the icosahedron (Ih), decahedron (Dh), and cuboctahedron (Co). While, less frequently, they may adopt the aCo or a hexagonal close-packed (hcp) geometries. These NP architectures are all reported in Figure 1. Ag and Pt present a small size mismatch, less than 4%, and they exhibit a large immiscibility gap in the bulk. Taking into account that Ag has a lower surface energy and a larger radius than Pt, for a 2:1 composition a perfect core-shell, $Ag_{92}^{shell}Pt_{55}^{core}$, is found.[35] At 1:1 composition ratio, $Ag_{74}^{surface}Pt_{73}$ the core is still made of Pt and Ag is only at surface while the shell is randomly mixed.

We perform classical molecular dynamics (MD) simulations, coupled with metadynamics, where a velocity Verlet algorithm is used to solve Newton's equations of motion. A time step of 5 fs is considered and the temperature is controlled via an Andersen thermostat. Atomic interactions are modelled within the second moment approximation of the tight binding theory[36] (TBSMA), where the potential $V_{TBSMA}(r_{ij})$ depends on the set of all atomic coordinates r_{ij} and is the sum of atomic contributions, E^i_{TBSMA},

$$E^i_{TBSMA} = \sum_{j\neq i}^{n_v} A_{ab} e^{-p_{ab}\left(\frac{r_{ij}}{r^0_{ab}}-1\right)} - \sqrt{\sum_{j\neq i}^{n_v} \xi^2_{ab} e^{-2q_{ab}\left(\frac{r_{ij}}{r^0_{ab}}-1\right)}}. \tag{1}$$

Here, the sum is extended up to the number of atoms n_v within an appropriate cut-off distance from atom i; a and b refer to the chemical species of the two atoms, r^0_{ab} is the bulk nearest neighbour distance for the homometallic atomic pair and their arithmetical average for the bimetallic case. A_{ab} and ξ_{ab} are related to the cohesive energy, while p_{ab} and q_{ab} and their product tune the range of the repulsive and of the attractive part of the potential. Details of their parametrisation and their values for Ag and Pt are reported in Ref. 37 while for AgPt, parameters are taken from Ref. 35.

MetaD enables the enhanced sampling of the free energy landscape of a system. It couples a coarse grained description of the system dynamics in the collective variables space to an history-dependent biasing potential, ΔV, which evolves as the sum of Gaussians of height ω and width σ added every t_G time interval,

$$V(r_{ij}) = V_{TBSMA}(r_{ij}) + \Delta V\left(S(r_{ij}),t\right),$$
$$\Delta V\left(S(r_{ij}),t\right) = \sum_{t'=t_G,2t_G\ldots} \omega e^{-\frac{\left[S(r_{ij})-s(t')\right]^2}{2\sigma^2}}. \tag{2}$$

$S(r_{ij})$ represents the set of collective variables chosen and defines the order parameter space where the MetaD potential evolves; $s(t')$ is the value of the collective variable at time t'. The efficiency and physical faithfulness of MetaD are strongly related to the choice of the CV set. The metric described by the chosen CVs should be able to distinguish between the various configurations the system can visit. The CV set should also be representative of all slow degrees of motions involved in the structural transformations of interest. Furthermore, the number of CVs should be limited in order to explore a low dimensionality space, hence avoiding undesired computational expenses. If one of the above conditions is not fully respected, the system may be forced to visit high energy configurations and processes of interest may be hidden.[15] When the MetaD exploration reaches a diffusive regime, the FES projection in the CV space can be reconstructed as the negative of the MetaD potential $\Delta V(S(x),t)$ in Eq. (2).

In cluster physics, the research of a good order parameter able to differentiate among the various isomers is not trivial.[38,39] We have noted that an almost complete information on NP morphology is encoded in its pair distance distribution function (PDDF), as depicted in Figure 2. We choose our CV set according to the following criterion: it must be able to distinguish the most common structures a metallic nanocluster can form, shown in Figure 1. Thus, we introduce specifically tailored order parameters corresponding to a window function (WF) on the PDDF constructed via a sigmoid function,

$$WF(x) = \sum_{i,j;i\neq j} \frac{1-\left(\frac{r_{ij}-d_0}{r_0}\right)^6}{1-\left(\frac{r_{ij}-d_0}{r_0}\right)^{12}}, \tag{3}$$

where r_{ij} is the distance between the ith and jth atoms, r_0 the window width, always set to 0.05 times the bulk lattice constant, and d_0 is the window function characteristic distance.

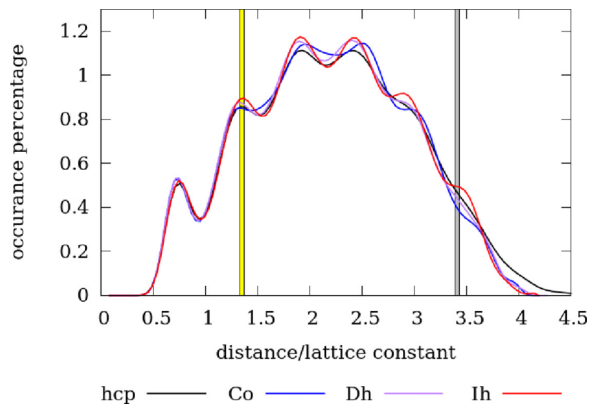

FIG. 2. Pair distance distribution function for icosahedral (orange), decahedral (blue), cuboctahedral (grey), and hcp (black) motifs of a 147 atom cluster. The selected windows around the stacking fault number (SFN) and the maximum pair distribution difference (MPDD) are highlighted in yellow and grey shadowing, respectively.

d_0 is set to be 1.354 and 3.4 of the bulk lattice parameter for the stacking fault number (SFN) and the maximum pair distance difference (MPDD), respectively, as highlighted in Figure 2.

A qualitative physical argument can be provided to support our choice. The SFN is related to a characteristic hcp peak in the PDDF. This is a topological defect obtained due to the intersection of two planes with different symmetry orientation. At the nanoscale, as in the bulk, phase transformations happen via stacking faults, as demonstrated for the DSD mechanisms in small Lennard-Jones clusters.[40] Consequently, a bias on this CV should not constrain the FES exploration to unphysical structural transitions and should represent the sliding and rotation of (111) planes, the slow degree of freedom in DSD mechanisms. The MPDD is centred where the pair distribution functions of the different geometries are less overlapping. In such a way, we are confident of being able to discriminate at least the morphologies of Figure 1.

We resort to the use of these two window functions on specific lattice distances because they adopt different values for each of the geometries of interest and are computationally cheap. This will enable us to easily extend our methodology to larger systems.[41] We note that a partial correlation of the two CVs may cause a small loss in accuracy however, this set of CVs appeared to be more robust than others based on coordination numbers or three-bodies quantities.[41] We remark that this set of CVs can be applied with a partial confidence to bimetallic nanoalloys. As the different chemical species are not treated explicitly, a complete chemical reordering transformation may be difficult to be reproduced biasing on these two CVs. However, as we focus on a stable $Ag^{shell}Pt^{core}$ ordering, SFN and MPDD capture several geometrical structural transitions.

NP geometrical features are monitored on-the-fly via common neighbour analysis (CNA).[42] The CNA associates to the local network of each nearest neighbour atom pair a signature made of three integers (r,s,t). r is the number of common nearest neighbours, s the number of bonds between the r-common nearest neighbours, and t is the longest chain among the s-bonds. CNA signatures are able to distinguish whether a pair of atoms belongs to a bulk environment ($s \geq 4$), to a facet ($s = 2,3$), to a FCC bulk ((4,2,1) signature), to a fivefold axis ((5,5,5) signature), or lies between two grain boundaries ((4,2,2) signature). Any isomer is characterised by a typical percentage value of a few signatures. The polyhedra considered in Figure 2 can be distinguished in terms of their (4,2,2) and the (5,5,5) signatures, illustrated in Figure 3. At 147 atoms, the (4,2,2) percentage decreases from 39% (Ih) to 25% (Dh and hcp) and zero (Co), while the (5,5,5) percentage ranges between 5.2% (Ih), 0.9% (Dh), and zero (Co and hcp).

A significant change in the CVs and in the CNA signatures is, therefore, distinctive of a structural transition, as in the paradigmatic example of $Ag_{92}^{shell}Pt_{55}^{core}$ sketched in Figure 4, where the three different basins, Ih (orange), Co (blue), and Dh (pink), are explored. Configurations involved in structural rearrangements are then quenched in order to identify precisely the initial, saddle, and final configurations. The lower panel of Figure 4 reports the quantity ΔE_{quench}, defined as the potential energy of a structure, rescaled with

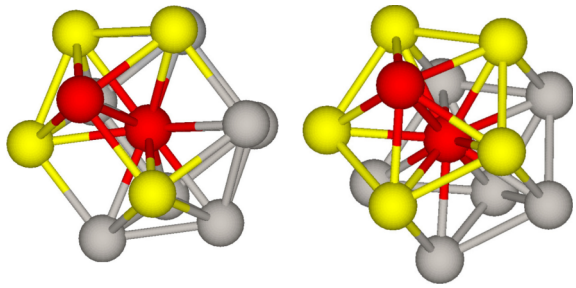

FIG. 3. Common neighbour network (yellow) of the red-coloured atomic pair considered. Left panel shows a (422) signature, associated with twin boundaries, while the right panel depicts a (555) signature, related to pairs lying on a 5-fold symmetry axis.

respect to the total energy of the Ih minimum E_{Ih}^{quench}, which results to be the most energetically favourable in all the considered systems. Potential energy barriers (PEBs) are then calculated by means of the DEPTS method, available in the OPTIM package,[11,43] where the relaxed structures obtained during a MetaD run serve as the initial and final configurations.

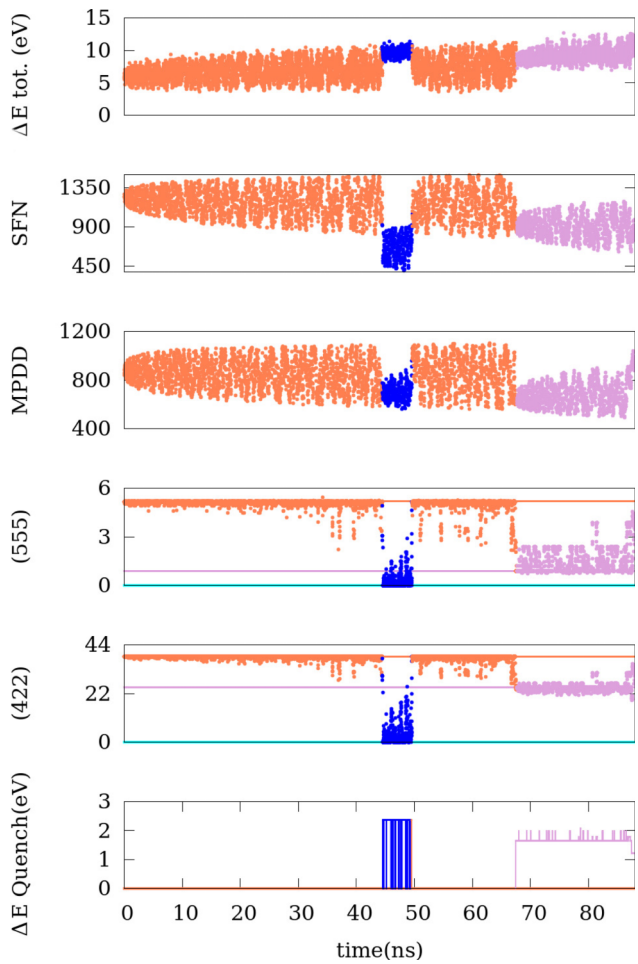

FIG. 4. $Ag_{92}^{shell}Pt_{55}^{core}$ MD + MetaD simulation outcome and analysis. From top to bottom: total energy difference ($\Delta E_{tot} = E_{tot} - E_{Ih}^{quench}$), CV values, on-the-fly CNA signatures, total energy difference of relaxed structures taken from the simulation ($\Delta E_{quench} = E_{quench} - E_{Ih}^{quench}$). A colour scheme is applied to discriminate the independent conformations basin explored: Co-basin in blue, Ih-basin in orange, Dh-basin in pink.

III. RESULTS AND DISCUSSION

All the results shown in the following have been obtained at 300 K. Gaussians 0.25 eV high are deposited with a period of 20 ps. Their width, σ, is 15 along the SFN and 10 for the MPDD. Such values are based on the standard deviations of the CV during unbiased molecular dynamics simulations at 300 K and are chosen to ensure an efficient conformational flooding.

A. Solid-solid structural transformation pathways

The calculated solid-solid transformation mechanisms from Ih to Dh, Co and aCo basins, and vice versa are reported in Figures 5–7, respectively. The motion of atoms of a (111) facets is clearly identified via the different coloring while the initial, saddle, and final configurations are shown. As expected, they correspond to one of the DSD mechanisms predicted by Mackay.[33] Further, we highlight that the MetaD transition pathways obtained for monometallic systems are identical to the one obtained via OPTIM/DETPS.

A DSD mechanism consists of a stretching and rotation of triangular facets into a diamond first and then to a square by a collective screw dislocation of atoms. The dislocation corresponds to a rotation of different angles according to the initial and the final configurations. Conversely, a squared facet can transform into two triangular facets by the opposite movement. Five parallelograms are involved in the collective rearrangement Dh ↔ Ih (Figure 5) and six in the case of the Co ↔ Ih (Figure 6) and of an aCo ↔ Ih (Figure 7).

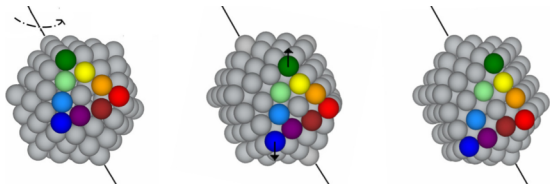

FIG. 5. Initial, saddle, and final configurations of DSD mechanism for Ih into Dh transformation. Multicolored atoms delimit a facet in the original Ih. Rotation along the depicted axis is of 36°.

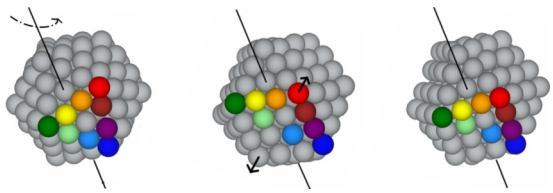

FIG. 6. Initial, saddle, and final configurations of DSD mechanism for Ih into Co transformation. Multicolored atoms delimit a facet in the original Ih. Rotation along the depicted axis is of 60°.

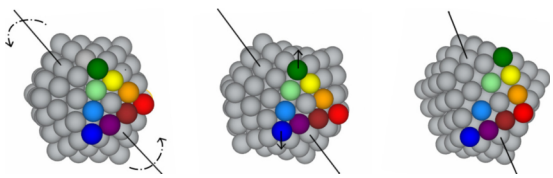

FIG. 7. Ih transforming into aCo via DSD mechanism. Saddle point is pictured in between the two. Multicolored atoms delimit a facet in the original icosahedron which turns into a diamond one by rotating by 60 in opposite direction with respect to the parallel triangular facet.

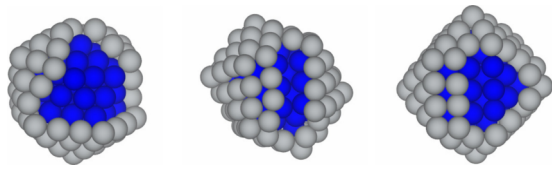

FIG. 8. Initial, saddle, and final configurations in the case of Dh into Ih transformation in $Ag^{92}_{shell}Pt^{core}_{55}$. Ag atoms are in grey, Pt in blue. Few atoms from Ag shell are removed to show Pt inner core.

An aCo can convert into an Ih throughout a rotation in opposite ways of the two triangular facets perpendicular to the aCo three-fold rotation axis, by 60° with reference to each other, along the same axis. The difference with the six DSD mechanisms between Co ↔ Ih is that now two opposite parallel triangular facets rotate about their normal and three pairs of abutting triangular facets remain unchanged, rotating about the axis that is perpendicular to their common edge and belongs to the twin plane. To our knowledge, this is the first time Mackay's path has been found in a numerical simulation.

No other mechanism appears to be able to connect the Ih and Co, Ih and aCo and Ih to Dh. Also, the solid-solid transition pathways for perfect core-shell ordering are identical to the one earlier described. It is important to note that the transition happens simultaneously in the two chemical species, as shown in Figure 8.

For $Ag^{surface}_{74}Pt_{73}$, a few transitions as a Dh into Ih, and an Ih into a defected Co have been reproduced. We note that in this system structural rearrangements involve both DSD and surface reconstruction mechanisms as depicted in Figure 9. Further studies are then needed in order to fully understand the interplay between the collective geometrical mechanism and the atomic inter-diffusion.

B. Energy landscapes analysis

In this subsection, we will discuss the reconstruction of the free energy landscapes for the various systems. Significance of entropic effects at 300 K will also be addressed via a comparison between free energy and potential energy barriers, when possible. We dedicate a paragraph to each system considered. In Ag_{147}, the Ih, Co, and the aCo basins exploration reaches a diffusive regime, we also observed the Dh conversion into an Ih, but the opposite transition has not been visible. In the case of the Pt_{147} clusters, only the transformations into an Ih geometry from Dh Co, and aCo

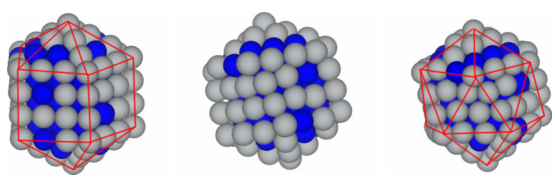

FIG. 9. Initial, saddle, and final configurations in the case of Dh into Ih transformation in $Ag^{surface}_{74}Pt_{73}$. Ag atoms are in grey, Pt in blue. Red lines highlight facets evolution in structural rearrangement process.

basins have been observed before the exploration of highly defected structures. For $Ag_{92}^{shell}Pt_{55}^{core}$, the transformation Co into Ih and Dh into Ih have been detected together with their inverse processes. On the other hand, only the conversion from the aCo into the Ih basin has been seen.

1. Ag_{147}

For the Co → Ih (Co ← Ih) interconversion, the FEB is of 0.4 eV (3.2 eV). In the case of aCo → Ih (aCo ← Ih) transformation, it is of 0.5 eV (3.0 eV). The value of the same processes evaluated via DEPTS result, respectively, of 0.5 eV (3.2 eV) for the Co → Ih and of 0.64 eV (3.49 eV) for the aCo → Ih structural rearrangements.

In the case of the Dh to Ih conversion, the inverse structural transition has not been observed. We introduced a non-canonical approach to obtain an (over)estimate of the Dh→Ih FEB. In this case, the non-convergence is likely caused by the fact that defected Ih structures, e.g., rosette-like,[44] overlap and hide the Dh basin. However, the quantities in our on the fly geometrical analysis, CNA and ΔE_{quench}, can be used as additional order parameters to identify precisely when the FEB around the Dh basin have been overcome and the Ih basin exploration has started. The free energy landscape may be then reconstructed as the inverse of the MetaD potential needed to exit from the initial Dh basin to explore the Ih one. We approximate the free energy barrier to the highest energy point in that landscape. Following this scheme, the Dh → Ih free energy barrier is (over)estimated to be of 0.6 eV. Error on our overestimate may be heuristically taken to be at least equal to the height of one Gaussian (0.25 eV). Activation barrier for the Dh → Ih transition calculated via DEPTS is of 0.45 eV and 2.17 eV for the direct and inverse process, respectively. In the case of the fully converged Ih ↔ Co and Ih ↔ aCo, the entropic contribution calculated as the difference between FEB and PEB is of the order of 0.1 eV. If we consider a similar entropic effect on the Dh → Ih process, the calculated upper bound and relative error for the estimate of that free energy barrier results sensible.

2. Pt_{147}

In this system, only rearrangements from Dh, Co, and aCo to Ih have been simulated. Exploration starting from Ih basin led only to defected geometries. The system remains trapped into the large Ih conformational basin and convergence cannot be reached in a reasonable time. Our CVs in fact do not hinder the transformation in defected geometries which might overlap the Dh or Co-basin. We recall that Pt_{147} shows a strong tendency to form Ih defected structure, related to its ability to reconstruct facets as described in Ref. 44, which appear to be entropically favourite even with respect to the perfect Ih structure at high temperatures. This may be the physical origin that prevents the system to reach a diffusive regime between the perfect geometry conformations.

Then, FEBs have been estimated within the non-conventional approach described in Sec. III B 1. They result in 1.9 eV for Dh → Ih, 1.7 eV for Co→Ih, and 2.07 eV for aCo→Ih, while the corresponding PEB values are of 2.11 eV, 1.9 eV, and 1.87 eV, respectively. Notwithstanding the non-conventional estimate of the FEB, barriers for Co-Ih and Dh-Ih transition result slightly lower than PEB ones, in a similar fashion to the one calculated for the converged Ag runs. If we take into account that the structural rearrangement pathways from MetaD and DETPS algorithms are almost identical, and assume that the entropic effects in Ag and Pt systems may be comparable, this makes us confident that the CVs employed are actually sensible and that our free energy barrier estimates are reasonable.

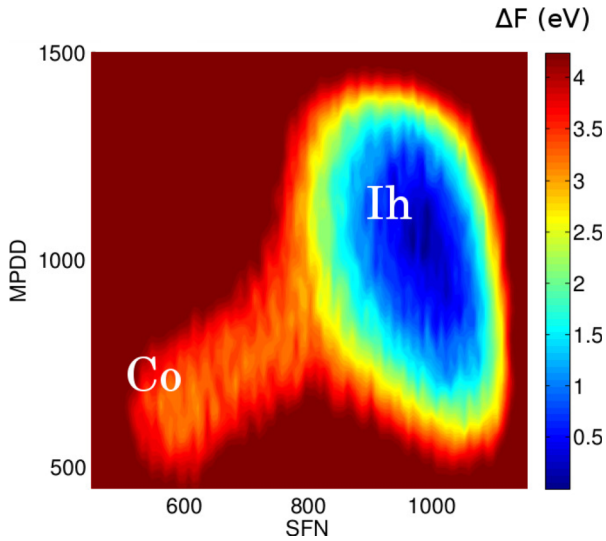

FIG. 10. Co and Ih basin free energy surface reconstruction for a $Ag_{92}^{shell}Pt_{55}^{core}$. Hot colours in the CV space highlight a high free energy of the corresponding configuration.

3. $AgPt_{147}$

In the case of the Co ↔ Ih transformation in $Ag_{92}^{shell}Pt_{55}^{core}$, the calculated FEB is 0.25 eV and 3.6 eV, respectively. The details of this MetaD run are reported in Figure 4 and the FES reconstruction is shown in Figure 10. Roughness of the landscape can be bestowed to the sampling of intermediate defected structures. A small barrier for escaping the Co-basin may be related to the fact that this shape is energetically unfavourable.

The Dh into Ih runs are also convergent but a partial basin overlap appears due to the exploration of a wide number of defected structures, thus causing a significant underestimation of the free energy barrier if the standard approach is used. Hence, we again adopt the FEB upper bound evaluation previously described. The upper bound of the Dh → Ih (Dh ← Ih) transition is of 1.5 eV (4.3 eV).

The energy barriers for the Dh-Ih core-shell structural rearrangement processes are in between the ones found for pure Ag and pure Pt clusters. Co-Ih and aCo-Ih barriers in $Ag_{92}^{shell}Pt_{55}^{core}$ appear smaller than the one calculated for monometallic systems as these configurations are essentially not energetically stable.

FEB investigation for $Ag_{74}^{surface}Pt_{73}$ is discouraged by the non diffusivity of the simulation, by the fact that the structural rearrangement pathway is more complex with respect to the

other system, and by the simple fact that they will depend on the arbitrarily initial distribution of Pt and Ag atoms in the uppermost layer.

IV. CONCLUSION

We have demonstrated how standard metadynamics can be adapted to the study of solid-solid structural transitions in metallic and bimetallic nanoparticles by introducing specific collective variables. These are two window functions centred on the pair distance distribution function, where they refer to the stacking fault number and the maximum pair distribution distance among different closed shell polyhedra. We remark that our set of collective variables can be applied to monometallic (e.g., Ag, Pt) and bimetallic systems with a small mismatch (e.g., AgPt) and with a stable core-shell chemical ordering. We want to highlight that in nanoalloys with a large mismatch, a limitation to the use of this set of CVs occurs: a broadening of the peaks in the PDDF may result in the impossibility of uniquely defining the characteristic distances in the window functions (Eq. (3)).

We have shown that the solid-solid structural transitions among the most common structural motifs happen following the Lipscomb's diamond-square-diamond mechanism, which is a collective screw dislocation motion. Further, we have demonstrated that the Mackay's description of the interconversion of an Ih into an aCo throughout a DSD mechanism is reproducible. According to our *in silico* experiments, structural rearrangement mechanisms that allow to connect minima on the free energy surface are identical to the one on the potential energy landscape. We would like to remark that the DSD mechanism appears to be a universal pathway as it takes place in monometallic as well as in nanoalloys with a small either non negligible mismatch, such as in AgAu[45] and AgPt, this work.

Finally, entropic effects appear to play a minor role at room temperature as the calculated free energy barriers are comparable in magnitude to the activation energy ones. We acknowledge that the overestimate of our methodology may be compensating for some of the entropic effects which would reduce further the magnitude of the free energy barriers. Further, we notice that Ih and Dh basins overlap in the considered CV space due to the exploration of defected Ih structures, which may hide the Dh basin.

ACKNOWLEDGMENTS

L.P. and F.B. thank the financial support by U.K. research council EPSRC, under Grant Nos. EP/GO03146/1 and EP/J010812/1. K.R. acknowledges financial support by U.K. research council EPSRC, Grant No. ER/M506357/1. The simulations were carried out using Departmental computational facilities at King's College London.

[1]R. Ferrando, J. Jellinek, and R. L. Johnston, Chem. Rev. **108**, 845 (2008).
[2]F. Baletto and R. Ferrando, Rev. Mod. Phys. **77**, 371 (2005).
[3]D. J. Wales and P. Salamon, Proc. Natl. Acad. Sci. U. S. A. **111**, 617 (2014).
[4]A. S. Barnard and P. Zapol, J. Chem. Phys. **121**, 4276 (2004).
[5]R. S. Berry and B. M. Smirnov, Phys.-Usp. **48**, 345 (2005).
[6]Z. H. Li and D. G. Truhlar, Chem. Sci. **5**, 2605 (2014).
[7]Z. W. Wang and R. E. Palmer, Phys. Rev. Lett. **108**, 245502 (2012).
[8]C.-C. Chen, C. Zhu, E. R. White, C.-Y. Chiu, M. C. Scott, B. C. Regan, L. D. Marks, Y. Huang, and J. Miao, Nature **496**, 74 (2013).
[9]E. Ringe, R. P. V. Duyne, and L. D. Marks, J. Phys. Chem. C **117**, 15859 (2013).
[10]G. Henkelman and H. Jo, J. Chem. Phys. **113**, 9901 (2000).
[11]D. J. Wales, Mol. Phys. **102**, 891 (2004).
[12]F. Calvo, A. Fortunelli, F. Negreiros, and D. J. Wales, J. Chem. Phys. **139**, 111102 (2013).
[13]P. G. Bolhuis, D. Chandler, C. Dellago, and P. L. Geissler, Annu. Rev. Phys. Chem. **53**, 291 (2002).
[14]A. Laio and M. Parrinello, Proc. Natl. Acad. Sci. U. S. A. **99**, 12562 (2002).
[15]A. Laio and F. L. Gervasio, Rep. Prog. Phys. **71**, 126601 (2008).
[16]E. Darve, D. Rodríguez-Gómez, and A. Pohorille, J. Chem. Phys. **128**, 144120 (2008).
[17]G. Torrie and J. Valleau, J. Comput. Phys. **23**, 187 (1977).
[18]D. J. Earl and M. W. Deem, Phys. Chem. Chem. Phys. **7**, 3910 (2005).
[19]G. Adjanor, M. Athènes, and F. Calvo, Eur. Phys. J. B **53**, 47 (2006).
[20]J. P. Neirotti, F. Calvo, D. L. Freeman, and J. D. Doll, J. Chem. Phys. **112**, 10340 (2000).
[21]F. Calvo and C. Mottet, Phys. Rev. B **84**, 035409 (2011).
[22]F. Calvo, J. P. K. Doye, and D. J. Wales, Nanoscale **4**, 1085 (2012).
[23]F. Calvo and E. Yurtsever, J. Chem. Phys. **140**, 214301 (2014).
[24]E. G. Noya and J. P. K. Doye, J. Chem. Phys. **124**, 104503 (2006).
[25]C. Bealing, R. Martonák, and C. Molteni, J. Chem. Phys. **130**, 124712 (2009).
[26]C. Bealing, R. Martoák, and C. Molteni, Solid State Sci. **12**, 157 (2010).
[27]D. Bochicchio *et al.*, J. Chem. Phys. **140**, 2024911 (2014).
[28]J. Liu and Q. Ge, J. Phys.: Condens. Matter **23**, 345401 (2011).
[29]F. Pietrucci and W. Andreoni, Phys. Rev. Lett. **107**, 85504 (2011).
[30]G. A. Tribello, J. Cuny, H. Eshet, and M. Parrinello, J. Chem. Phys. **135**, 114109 (2011).
[31]G. Santarossa, A. Vargas, M. Iannuzzi, and A. Baiker, Phys. Rev. B **81**, 174205 (2010).
[32]L. Pavan, C. Di Paola, and F. Baletto, Eur. Phys. J. D **67**, 24 (2013).
[33]A. L. Mackay, Acta Crystallogr. **15**, 916 (1962).
[34]W. N. Lipscomb, Science **153**, 373 (1966).
[35]L. O. Paz-Borbón, R. L. Johnston, G. Barcaro, and A. Fortunelli, J. Chem. Phys. **128**, 134517 (2008).
[36]V. Rosato, M. Guillopé, and B. Legrand, Philos. Mag. A **59**, 321 (1989).
[37]F. Cleri and V. Rosato, Phys. Rev. B **48**, 22 (1993).
[38]D. J. Wales, J. Chem. Phys. **142**, 130901 (2015).
[39]F. Pietrucci and R. Martoák, J. Chem. Phys. **142**, 104704 (2015).
[40]J. Uppenbrink and D. J. Wales, Faraday Trans. **87**, 215 (1991).
[41]L. Pavan, "Structural transformation in metallic nanoparticles," Ph.D. thesis, NMS School–King's College London, 2015.
[42]J. D. Honeycutt and H. C. Andersen, J. Phys. Chem. **91**, 4950 (1987).
[43]S. Trygubenko and D. Wales, J. Chem. Phys. **120**, 2082 (2004).
[44]E. Aprà, F. Baletto, R. Ferrando, and A. Fortunelli, Phys. Rev. Lett. **93**, 65502 (2004).
[45]F. Chen and R. L. Johnston, Appl. Phys. Lett. **92**, 023112 (2008).